Check for updates

View Article Online
View Journal

PCCP
Physical Chemistry Chemical Physics

Accepted Manuscript

This article can be cited before page numbers have been issued, to do this please use: S. Karbalaei Khani, B. Geissler, E. Engelage, P. Nuernberger and C. Hattig, *Phys. Chem. Chem. Phys.*, 2021, DOI: 10.1039/D1CP00009H.



This is an Accepted Manuscript, which has been through the Royal Society of Chemistry peer review process and has been accepted for publication.

Accepted Manuscripts are published online shortly after acceptance, before technical editing, formatting and proof reading. Using this free service, authors can make their results available to the community, in citable form, before we publish the edited article. We will replace this Accepted Manuscript with the edited and formatted Advance Article as soon as it is available.

You can find more information about Accepted Manuscripts in the Information for Authors.

Please note that technical editing may introduce minor changes to the text and/or graphics, which may alter content. The journal's standard Terms & Conditions and the Ethical guidelines still apply. In no event shall the Royal Society of Chemistry be held responsible for any errors or omissions in this Accepted Manuscript or any consequences arising from the use of any information it contains.

View Article Online
DOI: 10.1039/D1CP00009H

PCCP

ARTICLE TYPE

Cite this: DOI: 00.0000/xxxxxxxxxx

Tracing Absorption and Emission Characteristics of Halogen-bonded Ion Pairs Involving Halogenated Imidazolium Species†

Sarah Karbalaei Khani,*[a] Bastian Geissler,[b] Elric Engelage[c], Patrick Nuernberger*[b‡] and Christof Hättig*[a¶]

Received Date
Accepted Date

DOI: 00.0000/xxxxxxxxxx

We investigate how the absorption and fluorescence of halogenated imidazolium compounds in acetonitrile solution is influenced by the presence of counterions and the ability to act as halogen-bond donors. Experimental measurements and quantum chemical calculations with correlated wavefunction methods are applied to study three monodentate halogen-bond complexes of iodo-imidazolium, iodo-benzimidazolium and bromo-benzimidazolium cations with triflate counterions, and a bidentate complex of bis(iodo-benzimidazolium) dications with chloride as counterion. The three monodentate complexes with triflate counterions relax after photoexcitation to minima on the S_1 potential energy surface where the C–I bond and the I···O halogen bond are partially broken. For the bidentate complex with the smaller chloride counterion the halogen-bond interaction stays intact in the S_1 minimum that is reached by relaxation from the Franck-Condon point. In a complementing experimental approach, stationary absorption and emission as well as transient fluorescence spectra are recorded for iodo- and bromo-benzimidazolium in acetonitrile. Variation of the counterion, substitution of the iodine by bromine, hydrogen, or methyl, and the comparison to theory allows the identification of spectroscopic signatures and photoinduced dynamics associated with ion-pairing.

1 Introduction

A halogen bond (XB) is a non-covalent interaction between the σ-hole (an electron charge depletion region) in the anisotropic charge distribution of covalently bound halogen atoms and a Lewis base. The effects of halogen bonding have been extensively studied *e.g.* in the field of engineering of crystals[1] or liquid crystals[2] and there are also several theoretical studies of XB complexes in vacuum[3–5]. However, several aspects of this interaction in solution are not yet fully understood[6,7] despite its importance for many applications *e.g.* in organocatalysis and molecular recognition.[8–11]

Theoretically, numerous groups have studied XB complexes with different *ab initio* methods and different energy decomposition schemes to clarify the relative importance of contributions from electrostatic, dispersion, polarization and charge transfer interactions.[5,12,13] In 2008, Riley *et al.* explored the interaction energies for XB halomethane-formaldehyde complexes with Hartree-Fock (HF), second-order Møller-Plesset perturbation theory (MP2), and coupled-cluster singles and doubles with a perturbative triples correction, CCSD(T).[3] Results from their study with symmetry-adapted perturbation theory (SAPT) showed that halogen bonds are dominated by electrostatic and dispersion forces. For example, for systems containing iodine as XB donor the electrostatic interaction accounts for more than half of the attractive contributions. An extensive survey of the wavefunction methods MP2, MP3, CCSD, and their spin-component scaled (SCS) counterparts along with CCSD(T) and density functional theory (DFT) for geometries and dissociation energies of XB complexes was carried out in 2013 by Kozuch *et al.*[4] Their benchmark results revealed that for dissociation energies of halogen bonds the wavefunction methods SCS-MP2 and CCSD(T) — if used with accurate basis sets — are on average more accurate than DFT because the latter has difficulties to provide a balanced description of the different contributions (electrostatic, dispersion, polarization, and charge transfer). Furthermore, they argued that, because of the overestimation of dynamic electron correlation, MP2 overbinds while SCS-MP2 provides more accurate results for dissociation energies which are predicted in the range of 1.4 kcal·mol^{-1} for weak and 10.1 kcal·mol^{-1} for strong halogen bonds.

[a] *Arbeitsgruppe Quantenchemie, Ruhr-Universität, Bochum 44780, Germany.*
[b] *Institut für Physikalische und Theoretische Chemie, Universität Regensburg, 93040 Regensburg, Germany.*
[c] *Organische Chemie II, Ruhr-Universität Bochum, 44780 Bochum, Germany.*

† Electronic Supplementary Information (ESI) available: tables with NTOs, transient fluorescence decay spectra, and time-resolved fluorescence streak images. See DOI: 10.1039/cXCP00000x/

‡ E-mail: patrick.nuernberger@ur.de
¶ E-mail: christof.haettig@rub.de

Published on 09 March 2021. Downloaded by Ruhr Universitat Bochum on 3/9/2021 10:47:03 AM.

Physical Chemistry Chemical Physics Accepted Manuscript

View Article Online
DOI: 10.1039/D1CP00009H

Published on 09 March 2021. Downloaded by Ruhr Universitat Bochum on 3/9/2021 10:47:03 AM.

Physical Chemistry Chemical Physics Accepted Manuscript

A challenge for the theoretical description of XB complexes in solution are the large solvent effects for ions which weaken the halogen bonding.[14–16]. This can change significantly the relative stability of different minima (*vide infra*).

Among the XB complexes used in organocatalysis are *e.g.* aromatic iodo(benz)imidazolium-based XB donors to activate hetero Diels-Alder reactions and dicationic bis(iodoimidazolium) compounds[17] to activate classical Diels-Alder reactions of enones with cyclopentadiene.[18–20] Due to the positive charge on the imidazolium moieties of iodo(benz)imidazolium compounds the halogen bond competes with an anion-π interaction between the anion (halogen bond acceptor) and the face side of the haloimidazolium ring. For instance, in a recent study by Huber *et al.* on the binding mode of 2-iodoimidazolium-based ion pairs in acetonitrile solution, the authors investigated the relative importance of XB and anion-π interactions for various imidazolium salts with bromide as counterion by sterically shielding potential bonding sites against hydrogen bonding and anion-π interactions as competitors for halogen bonding.[21] In general, stronger halogen bonds are obtained with bidentate XB donors. As an example for bidentate XB donors, Zapata *et al.* reported in 2012 a family of fluorescent bidentate chloro-, bromo-, and iodo-imidazoliophane donors. They showed that bromo-imidazoliophane and syn iodo-imidazoliophane exhibit strong and selective XB recognition of iodide and bromide anions, respectively.[22]

The aim of the current work is to gain insight into the effects of halogen bonding on electronic excitations. As model compounds for the computational investigations, we study the complexes of 2-iodoimidazolium (IIm^+), 2-bromobenzimidazolium ($BrBzIm^+$) and 2-iodobenzimidazolium ($IBzIm^+$) with the triflate (OTf^-) anion and the complex of a bis(2-iodobenzimidazolium) dication ($bIBzIm^{2+}$) with a chloride anion and compute for them the absorption spectra and the Stokes shifts for emitted fluorescent light in acetonitrile solution. The latter requires not only for the ground- but also for the excited-state potential energy surface a balanced account of the electrostatic and London dispersion interactions. This is difficult to obtain with time-dependent density functional theory (TDDFT). Therefore, we employ in the current study MP2 for the ground state in combination with the algebraic diagrammatic construction through second order, ADC(2), for the excitation energies and include solvent effects via the conductor-like screening model (COSMO).[23] To study the deexcitation mechanism we calculated the excited-state equilibrium structures in acetonitrile solution. For this we use a recently developed implementation of analytic excited-state gradients at the COSMO-ADC(2) level of theory.[24] To study the influence of halogen bonding on the excitation energies and the characters of the lowest excited states we carried out analogous calculations without counterions as XB acceptors. Experimentally, an XB may affect numerous observables of a molecule, with changes in transition energies and oscillator strengths being reflected in absorption and emission spectra. As known from other intermolecular interactions, *e.g.* the formation of hydrogen-bonded complexes[25–29], the dynamics following photoexcitation may provide further insight in addition to stationary measurements. In this way, characteristic signatures of the interaction may even be identified in cases where absorption spectra are virtually unchanged. With regard to halogen bonding, a time-resolved approach has very recently been pursued for intermolecular electron transfer processes[30,31] and the intersystem crossing rate of a dye capable of acting as XB donor[32].

Here, we will apply static absorption and transient fluorescence spectroscopy on 2-iodobenzimidazolium ($IBzIm^+$) with OTf^- or $[BAr_4^F]^-$ (tetrakis[3,5-bis(trifluoromethyl)phenyl]borate) counterions, respectively, and compare the results to reference systems without the possibility of XB formation. Differences in the corresponding fluorescence decay times are used to disclose the existence of complexes in acetonitrile solution and tests conclusions drawn from the theoretical studies *(vide infra)*.

2 Materials and Methods

Computational Methods For all three investigated systems the ground state structures in vacuum have been optimized at the MP2[33] level of theory using the doubly polarized triple-zeta basis def2-TZVPP[34] as orbital basis set combined with the corresponding optimized auxiliary basis sets for the resolution-of-the-identity (RI) approximation.[35] For iodine we used the Stuttgart-Cologne 28 electron effective core potential (ECP)[36]. The frozen core approximation was applied to all non-hydrogen atoms: for C, O, and N atoms the $1s^2$ electrons were kept frozen, for sulfur and chlorine in addition all electrons in the $2s^22p^6$ shell, and for bromine in addition also all electrons in the $3s^23p^6$ shell. For iodine we excluded (in addition to the electrons modeled by the ECP) also the electrons in the $4s^24p^6$ shell from the correlation treatment.

For the calculations in acetonitrile as solvent, the ground state structures have been optimized at the COSMO-MP2(PTE) level (PTE stands for the perturbation on energy scheme)[37] with the same basis sets as in vacuum.[23,38]. Vertical excitation energies, oscillator strengths, and the excited-state structures in vacuum were obtained at the RI-ADC(2)/def2-TZVPP level[39,40] and in acetonitrile with COSMO-RI-ADC(2)/def2-TZVPP within the post-SCF reaction field scheme using the implementation reported in Ref. 24.

All the Hartree-Fock, RI-MP2, and RI-ADC(2) calculations in vacuum were done with version V7.2 of the TURBOMOLE program package[41]. For the COSMO-RI-ADC(2) calculations we used a development version of the `ricc2` module of TURBOMOLE.[24,42] For the calculations in solution, acetonitrile has been used throughout as the solvent with a dielectric constant of $\varepsilon = 36.7$ and a refractive index of $n=1.345$.

Experimental Methods 2-iodo- and 2-bromo-N-methylbenzimidazole were synthesized[43] according to literature.[44,45] Subsequently the compounds were treated with 1 eq of methyl triflate in dry acetronitrile at room temperature, stirred for one hour, precipitated and washed with a small amount of dry diethyl ether to yield the pure triflate salts.[45] The triflate $[BAr_4^F]^-$ exchange was performed according to literature using $NaBAr_4^F$ and chloroform as solvent.[44,46] The precipitated NaOTf was filtered off and the residue was covered with cyclohexane to grow $IBzImBAr_4^F$ crystals.

All samples were prepared with spectroscopic-grade acetonitrile and a concentration of 390 μM. The experiments were car-

View Article Online
DOI: 10.1039/D1CP00009H

Published on 09 March 2021. Downloaded by Ruhr Universitat Bochum on 3/9/2021 10:47:03 AM.

Physical Chemistry Chemical Physics Accepted Manuscript

ried out with a Starna flow cell of type 48-Q-0.2 made of fused silica, with an optical path length of 0.2 mm and a sample volume of >15 mL. Absorption spectra were recorded on a V-770 UV-visible/NIR JASCO instrument and the steady-state fluorescence measurements on a FP-8300 JASCO spectrometer. For the time-resolved fluorescence experiments, the samples were excited by a laser (PicoQuant LDH-P-FA-266, 266(3) nm, repetition rate 40 MHz, pulse duration <80 ps FWHM) and the emitted fluorescence was sent via a monochromator (Princeton Instruments SP2150i) to a streak camera (Hamamatsu C10627-11).[47,48] For the transient fluorescence data, the sample was excited for 300 s. For halogenated compounds, additionally the cuvette was moved by a motor to not always excite the same sample volume; in this way, photodegradation during the measurement of the transient fluorescence data is precluded. For the non-halogenated compounds, the measurement time was 500 s. The polarization directions of pump laser and detected fluorescence, respectively, were linear and set to the magic angle.[47–49] The overall fitted instrument response function had a FWHM of 150 ps. The transient data was globally analyzed using TIMP[50] and characteristic decay times of the fluorescence dynamics are presented together with the corresponding decay-associated spectra (DAS).[51,52] The error on the fitted time constants is on the order of a few percent.

3 Computational Results

4 2-Iodo-imidazolium·OTf

An initial search for the ground state equilibrium structures of the complex formed by a 2-iodoimidazolium cation (IIm^+) and a triflate anion (OTf^-) in vacuum and in acetonitrile solution revealed two minima: the XB structure (S_0-eq), Fig. 1a, and a structure with an anion-π interaction between the positively charged imidazolium ring and the OTf^- counterion (S_0'-eq), Fig. 1c. At the MP2/def2-TZVPP level the anion-π structure in vacuum is predicted to be 12.6 kcal·mol^{-1} and in acetonitrile still 1.6 kcal·mol^{-1} below the XB structure. This is explained by the stronger electrostatic interaction in vacuum, which is partially screened in acetonitrile solution. In addition the dispersion interaction between the ions competes in solution with the dispersion interactions between the solvent and the ions. However, the COSMO solvation model does not account for the dispersion interaction between the quantum mechanically described solute and the solvent. This interaction should in solution weaken the stability of the anion-π structure (with a larger dispersion contribution to its binding energy) relative to the XB complex, so that MP2 probably overestimates the stability of the anion-π complex. To avoid this imbalance, we performed a second set of geometry optimizations at the B3-LYP/def2-TZVPP level[53] (without a dispersion correction[54]). This changes the energy difference in favor of the XB complex and makes it more stable than the anion-π complex by $\approx$ 2.77 kcal·mol^{-1} in acetonitrile solution. In vacuum the anion-π complex is still $\approx$ 7.08 kcal·mol^{-1} lower in energy, which means that in solution the XB structure should be dominant.[55] The geometry optimization at the COSMO-B3-LYP/def2-TZVPP level without dispersion correction gives a ground state equilibrium structure where, relative to the COSMO-MP2/def2-TZVPP(PTE) results, the I···O distance of the XB complex in solution stays essentially unchanged at 2.08 Å while the C–I bond length becomes longer by 0.04 Å.

Since our aim is to investigate the effect of the halogen-bond interaction on electronic spectra and excited states, we targeted the XB structure as the ground state geometry for the subsequent calculations. The vertical excitation energies and oscillator strengths for the five lowest excited states at the S_0-eq structures in vacuum and in acetonitrile solution were computed with ADC(2). The results for the XB complex in acetonitrile are summarized in Fig. 2 along with the natural transition orbitals (NTOs) associated with each electronic transition. Additional results for the complex in vacuum and IIm^+ in solution without counterion are given in Tables S1 and S2 of the supporting information (SI).

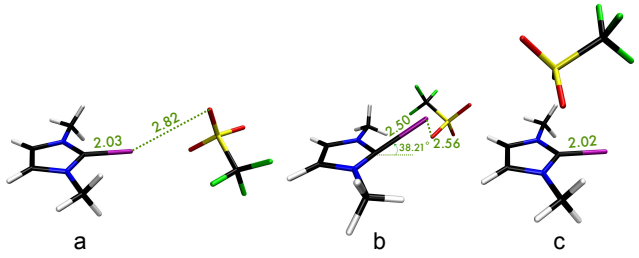


Fig. 1 Optimized geometries of IImOTf in (**a**) the ground state S_0-eq with XB interaction, (**b**) the first excited state S_1-eq and (**c**) the ground state S_0'-eq with an anion-π interaction. All structures have been computed in acetonitrile solution with COSMO-MP2/def2-TZVPP(PTE) for the ground state and COSMO-RI-ADC(2)/def2-TZVPP(post-SCF) for the excited state.

In contrast to vacuum, the polar solvent acetonitrile screens the Coulomb attraction between the ions and weakens their interaction. The stabilization of the charges by the polar solvent blue-shifts the charge transfer (CT) excitations from the lone pairs of iodine and OTf^- which decrease the polarity of the ion pair. The contributions from transitions out of the lone pairs of OTf^- to the lowest excitations become in acetonitrile solution insignificant (cmp. Fig. 2). Instead, the lowest excitations are in solution dominated by local transitions within the IIm^+ cation. As shown in Fig. 2, in acetonitrile solution from the two close-lying lowest excited states S_1 and S_2 only the S_1 state at 5.59 eV has a significant oscillator strength. It is a $\pi\pi^*$ transition, mostly localized on the iodoimidazolium ring with a partial charge transfer from the iodine atom into the ring. S_2 at 5.62 eV is a $\pi\sigma^*$ transition mainly from the iodine lone-pairs into the σ^* orbital of the C–I bond. The third excited singlet state at 6.34 eV with $n\sigma^*$ character from a lone pair of iodine to the σ^* orbital of the C–I bond and the S_4 and S_5 with $n\pi^*$ and $\pi\pi^*$ character have very small oscillator strengths and do not contribute to the UV absorption spectrum.

To evaluate the impact of the XB interaction on the absorption spectrum, we compared the results for the excitation energies and oscillator strengths of the XB complex and the cation without OTf^- counterion in Table 1.

Compared to the spectrum of the IIm^+ cation (cmp. SI Table S2), the $\pi\sigma^*$ and $n\sigma^*$ transitions into the antibonding orbital of the C–I bond are by the XB interaction blue-shifted by $\approx$ 0.56 and

View Article Online
DOI: 10.1039/D1CP00009H

Published on 09 March 2021. Downloaded by Ruhr Universitat Bochum on 3/9/2021 10:47:03 AM.

Table 1 Vertical excitation energies ΔE (eV) and oscillator strengths f of IImOTf complex and IIm^+ cation in acetonitrile at the COSMO-ADC(2)/def2-TZVPP(post-SCF) level

	IImOTf			IIm^+		
State	Type	ΔE	f	Type	ΔE	f
1	$\pi\pi^*$	5.59	0.437	$\pi\sigma^*$	5.06	0.000
2	$\pi\sigma^*$	5.62	0.005	$\pi\pi^*$	5.59	0.388
3	$n\sigma^*$	6.34	0.004	$n\sigma^*$	5.83	0.001
4	$n\pi^*$	6.59	0.000	$n\pi^*$	6.72	0.000
5	$\pi\pi^*$	6.84	0.000	$\pi\sigma^*$	6.95	0.000

0.51 eV. These transitions are, however, dark. The bright excitation of the cation into the lowest $\pi\pi^*$ state (S_2) appears at the same energy as in the XB complex *i.e.* at 5.59 eV. On the other hand, the S_4 state, which shows an $n\pi^*$ character for both, the XB complex and the cation, is red shifted by ≈ 0.13 eV in the presence of the XB interaction.

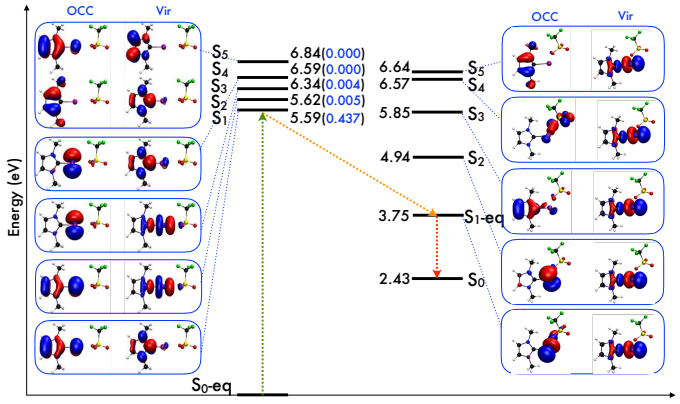


Fig. 2 IImOTf: Natural transition orbitals, vertical excitation energies (eV) (green arrow) and oscillator strengths (in blue) at the Franck-Condon geometry of the XB complex. A geometry optimization on the S_1 potential energy surface leads to S_1-eq (orange arrow). The emission energy (eV) at S_1-eq structure to S_0 is indicated by a red arrow. All excited-state results are at the COSMO-RI-ADC(2)/def2-TZVPP(post-SCF) level in acetonitrile solution. The ground-state geometry for S_0-eq was optimized at the COSMO-MP2/def2-TZVPP(PTE) level in acetonitrile.

In the gas phase, the unscreened Coulomb attraction between the IIm^+ cation and OTF^- leads to a strong XB interaction and large effects on the electronic transitions in the cation. The two lowest vertical transitions of the XB IImOTf complex in vacuum appear at 5.22 and 5.33 eV. These transition are bright and have mixed $n\pi^*$ and $\pi\pi^*$ characters (cmp. SI Table S1).

After photoexcitation of the IImOTf complex in acetonitrile solution and relaxation on the S_1 potential energy surface from the Franck-Condon point to the S_1-eq structure, where S_1 has a $\pi\sigma^*$ character, the C–I bond is elongated by about 0.47 Å to 2.50 Å and tilted out of the plane of the imidazole ring by ≈ 38°. The elongation of the C–I bond in the S_1-eq structure is accompanied by a reorientation of the OTf^- anion and, to some extent, a stronger XB interaction between iodine and an oxygen atom of OTf^- which causes a shortening of the I···O distance by 0.26 Å to 2.56 Å (cmp. Fig. 2). The reorientation of the halogen bond is triggered by the change of the character of S_1 into an $n\sigma^*$ transition from a lone pair of the iodine atom into the C–I antibonding orbital. This shifts the σ-hole away from the C–I bond axes.

The NTOs of the five lowest transitions at the S_1-eq structure show that these excitations are all either $n\sigma^*$ or $\pi\sigma^*$ transitions, mostly from iodine non-bonding orbitals into the σ^* orbital of the C–I bond, Fig. 2. The electronic deexcitation of the XB complex from S_1 into S_0 at the S_1-eq geometry emits ≈ 1.32 eV energy which can lead to a fast decay of the excitation without observable fluorescence. This emission energy is ≈ 1.26 eV lower than for the cation without XB counterion for which the deexcitation energy is 2.58 eV (cmp. SI Table S3). After the deexcitation to S_0, the relaxation of the complex on the ground state surface in solution does not lead back to the XB S_0-eq structure but rather to the S_0'-eq structure with an anion-π interaction between the positively charged imidazole ring and OTf^- which is energetically lower at the MP2 level.

The structural changes of the iodoimidazolium moiety along the relaxation on the S_1 surface are slightly larger for the XB complex than for the IIm^+ cation without counterion. In case of the cation, the C–I bond length at the S_1-eq structure is 2.45 Å, which is longer than the S_0-eq by 0.43 Å, and is tilted out of the plane of the imidazole ring by ≈ 31°.

The binding energy of OTf^- to the IIm^+ cation is in the ground state 6.9 kcal·mol^{-1} and increases in the excited state at the S_1-eq structure to 10.9 kcal·mol^{-1}. One can thus conclude that their interaction becomes stronger in the excited state at the S_1-eq structure due to the $n\sigma^*$ character of the transition.

5 2-Iodo- and 2-Bromobenzimidazolium·OTf

Also for the 2-iodobenzimidazolium·OTf (IBzImOTf) complex we found on the (COSMO-)MP2 ground state potential energy surface in vacuum and in acetonitrile solution two different minima, shown in Fig. 3a and c. As for IImOTf, due to the London dispersion interaction, the equilibrium structure with the anion-π interaction, Fig. 3c, is energetically more favorable than the XB minimum, in vacuum by ≈ 18.6 kcal·mol^{-1} and in acetonitrile solution at the COSMO-MP2 level still by ≈ 3.7 kcal·mol^{-1}. Again, to avoid the unbalanced treatment of dispersion interactions within the complex and between the complex and the solvent, we did in addition COSMO-B3-LYP/def-TZVPP calculations without dispersion correction in acetonitrile solution. This calculation predicts the anion-π complex by 1.2 kcal·mol^{-1} below the XB complex. Compared to the respective MP2 results, the I···O distance and the C–I bond length increased with DFT by 0.01 Å and 0.04 Å, respectively. In the 2-bromobenzimidazolium·OTf (BrBzImOTf) complex with the interaction energy of −5.4 kcal·mol^{-1}, the substitution of iodine with bromine reduces the energy gap between the XB (Fig. 3d) and π-stacking (Fig. 3f) minima at COSMO-MP2 level to 2.2 kcal·mol^{-1} in solution with the one with π-stacking interaction energetically lower. While at the COSMO-DFT level the stability order of these two isomers switches and predicts a lower total energy (by 2.1 kcal·mol^{-1}) for the XB isomer.

Since we are interested into the effects of the halogen bond on

Physical Chemistry Chemical Physics Accepted Manuscript

View Article Online
DOI: 10.1039/D1CP00009H

Published on 09 March 2021. Downloaded by Ruhr Universitat Bochum on 3/9/2021 10:47:03 AM.

the spectrum we again continued for IBzImOTf and BrBzImOTf with the XB structure. The results for the vertical excitation energies of IBzImOTf at the XB minimum and at the minimum on the S_1 surface which is reached from the Franck-Condon point in acetonitrile are summarized in Fig. 4. The results of similar calculations for the 2-iodobenzimidazolium ($IBzIm^+$) cation without close interaction with OTf^- and also of the XB BrBzImOTf complex and the $BrBzIm^+$ cation in solution are given in Table 2 and Tables S5, S7 and S9 of the SI, and for IBzImOTf in vacuum in Table S4 of the SI.

The extension of the π-system by a benzene ring decreases the energies of the unoccupied π-orbitals so that for the $IBzIm^+$ cation and its XB complex with OTf^-, the lowest singlet excitations, located at respectively 4.73 and 4.74 eV, are bright $\pi\pi^*$ transitions with a partial intra-molecular charge transfer from the iodine atom into the benzimidazole ring without direct contributions from orbitals of the counterion.

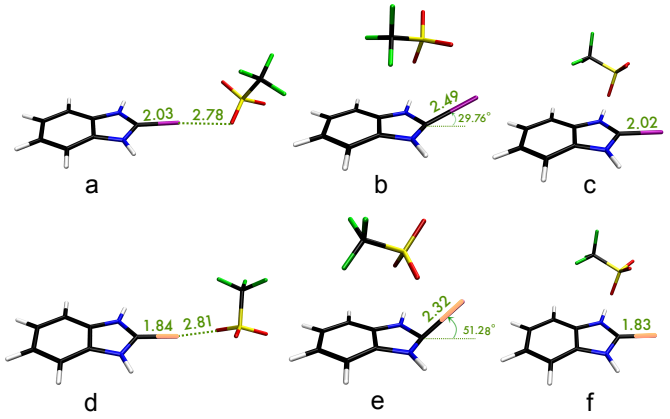


Fig. 3 Optimized geometries of IBzImOTf (upper row) and BrBzImOTf (lower row) in (**a, d**) the ground state S_0-eq with XB interaction, (**b, e**) the first excited state S_1-eq and (**c, f**) the ground state anion-π complexes S_0'-eq with an anion-π interaction. Iodine is colored purple and bromine salmon. All structures have been computed in acetonitrile solution with COSMO-MP2/def2-TZVPP(PTE) for the ground- and COSMO-RI-ADC(2)/def2-TZVPP(post-SCF) for the excited state.

As shown in Fig. 4, the next two lowest $\pi\pi^*$ states (S_2 and S_4) of the XB IBzImOTf complex in solution are located at 5.22 and 5.80 eV, respectively, with S_4 having significantly more intensity than S_2. Both are local transitions within the benzimidazolium moiety. Located between them is S_3, a dark $\pi\sigma^*$ transition into the σ^* orbital of the C–I bond. Also S_5 at 6.11 eV has no significant oscillator strength. This is a $n\pi^*$ transition from a nonbonding orbital of iodine into a π^* orbital localized mostly on the imidazolium moiety.

The interaction with OTf^- in the XB IBzImOTf complex increases the excitation energies for the lowest five transitions with the exception of S_1 which has in the XB IBzImOTf complex about the same excitation energy as in the $IBzIm^+$ cation without counterion. The second $\pi\pi^*$ transition for the XB complex at 5.22 eV corresponds to the S_3 state of the $IBzIm^+$ cation at 5.14 eV. But even more blue shifted in the XB complex is the $\pi\sigma^*$ transition into the antibonding σ^* orbital of the C–I bond, where the XB interaction increases the excitation energy from 5.10 eV to 5.67 eV.

Exchanging iodine with bromine in the XB BrBzImOTf complex rises the excitation energies for the three lowest $\pi\pi^*$ states by about 0.10 – 0.15 eV, while the excitation energy of the lowest $\pi\sigma^*$ state increases more significantly by ≈ 1.0 eV (cmp. Table 2). Similar to the BrBzImOTf complex, the lowest three $\pi\pi^*$ states (S_1, S_2 and S_3) of $BrBzIm^+$ appear at higher energies compared to its iodine counterpart (S_1, S_3 and S_5) by ≈ 0.1 eV. The S_4 state of $BrBzIm^+$ is a $\pi\sigma^*$ transition and has an excitation energy that is 1.08 eV higher than that of the analogous state (S_2) of $IBzIm^+$.

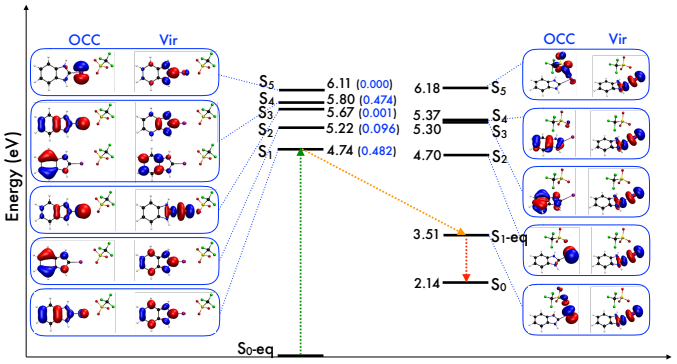


Fig. 4 IBzImOTf: Natural transition orbitals, vertical excitation energies (eV) (green arrow) and oscillator strengths (in blue) at the Franck-Condon geometry of the XB complex. A geometry optimization on the S_1 potential energy surface leads to S_1-eq (orange arrow). The emission energy (eV) at the S_1-eq structure to S_0 is indicated by a red arrow. All excited-state calculations are at COSMO-RI-ADC(2)/def2-TZVPP(post-SCF) level in acetonitrile solution. The ground-state geometry of S_0-eq was optimized at the COSMO-MP2/def2-TZVPP(PTE) level in acetonitrile.

For the XB IBzImOTf complex in the gas phase, S_1 is a $\pi\pi^*$ transition that is mainly localized on the iodobenzimidazolium moiety with partial CT out of the lone pairs of the iodine and the oxygen atoms of OTf^- to a π^* orbital of benzimidazolium. This transition at 4.55 eV is a bright state with an oscillator strength of 0.4. The S_2 state is a CT transition from oxygen lone pairs of OTf^- to the iodobenzimidazolium moiety at 4.67 eV.

To obtain the Stokes shift for the fluorescence emission, we optimized the geometry of the bright S_1 state of IBzImOTf and BrBzImOTf in acetonirile solution and determined the minimum reached from the Franck-Condon point of the XB complexes (S_1-eq) at the COSMO-RI-ADC(2)/def2-TZVPP level. The structures are shown in Fig. 3b and 3e and reveal that similar as in IImOTf, several internal coordinates change during the relaxation to the S_1-eq geometry: the CF_3 group of the OTf anion turns to the face side of the organic ring system which leads to an anion-π interaction similar as for the S_1-eq structure of IImOTf, the C–I bond lengthens by ≈ 0.46 Å and ≈ 0.48 Å and bends out of the molecular plane by ≈ 30° and ≈ 51° for IBzImOTf and BrBzImOTf, respectively. The lengthening of the C–I bond in the XB IBzImOTf and BrBzImOTf complexes with OTf^- is larger than for the $IBzIm^+$ and $BrBzIm^+$ cations without interaction with OTf^- by ≈ 0.09 Å and 0.032 Å, where at the S_1-eq minima of the cations this bond bends out of the molecular plane by ≈ 36° and 46°. Along the

Physical Chemistry Chemical Physics Accepted Manuscript

View Article Online
DOI: 10.1039/D1CP00009H

Table 2 Vertical excitation energies ΔE (eV) and oscillator strengths f of IBzImOTf and BrBzImOTf complexes and $IbzIm^+$ and $BrBzIm^+$ cations in acetonitrile at the COSMO-ADC(2)/def2-TZVPP(post-SCF) level.

	IBzImOTf			$IBzIm^+$			BrBzImOTf			$BrBzIm^+$		
State	Type	ΔE	f	Type	ΔE	f	Type	ΔE	f	Type	ΔE	f
1	$\pi\pi^*$	4.74	0.482	$\pi\pi^*$	4.73	0.445	$\pi\pi^*$	4.84	0.381	$\pi\pi^*$	4.84	0.350
2	$\pi\pi^*$	5.22	0.096	$\pi\sigma^*$	5.10	0.000	$\pi\pi^*$	5.27	0.124	$\pi\pi^*$	5.22	0.121
3	$\pi\sigma^*$	5.67	0.001	$\pi\pi^*$	5.14	0.093	$\pi\pi^*$	5.95	0.574	$\pi\pi^*$	5.95	0.496
4	$\pi\pi^*$	5.80	0.474	$n\sigma^*$	5.71	0.001	$\pi\sigma^*$	6.60	0.000	$\pi\sigma^*$	6.18	0.000
5	$n\pi^*$	6.11	0.000	$\pi\pi^*$	5.82	0.429	$\pi\pi^*$	6.73	0.046	$\pi\pi^*$	6.73	0.019

relaxation on the S_1 surface, the character of this state changes for both the XB complexes and the $IBzIm^+$cation, similar as for IImOTf, to a $n\sigma^*$ excitation from halogen non-bonding electrons into the antibonding σ^* orbital of the C–X bond (X= I, Br). For the $BrBzIm^+$ cation, at the S_1 equilibrium geometry an electron is transferring from a π orbital of the phenyl ring to the σ^* orbital of C–Br bond.

The emission energy at the optimized S_1-eq geometry from S_1 to S_0 is for the XB IBzImOTf complex with 1.37 eV approximately 1.2 eV lower than for the $IBzIm^+$ cation without XB interaction (cmp. SI Table S6). From IBzImOTf to BrBzImOTf the emission energy at the S_1-eq geometry decreases to 0.89 eV, while this energy for the $BrBzIm^+$ cation is very close to its iodine counterpart at 2.55 eV (cmp. Table S8 and S10 of the SI). Also similar as for IImOTf, the relaxation on the ground state potential energy surface starting from S_1-eq geometry for both iodine and bromine XB complexes leads to the S_0'-eq ground state structure, shown in Fig. 3c and 3f, with an anion-π interaction.

For the $BrBzIm^+$ cation we tested also the influence of methylation at the N atoms and of including explicit solvent molecules in the calculations. Both have only minor effects on the spectrum and the ground and excited state equilibrium structures (cmp. Tabs. S14 and S15 off the ESI). Substituting the H atoms bonded to the nitrogens by methyl groups decreases the vertical excitation energies to S_1 only marginal by 0.05 eV to 4.79 eV, the vertical fluorescence energy at the S_1 equilibrium structure is shifted a bit more by -0.27 eV to 2.28 eV. To test the importance of explicit solvent molecules we added in the electronic ground state an acetontrile molecule on top of the π-system and in front of the bromine atom (to test for a halogen-bond like interaction). In both positions the explicit solvent molecule did not lead to significant changes in the structure of the $BrBzIm^+$ cation and its lowest excitation energy at both the S_0 and the S_1 equilibrium geometries. Similar as with OTf^-, the halogen-bond like structure rearranges on the S_1 potential energy surface.

To investigate the deexcitation mechanism of the BrBzImOTF, intrinsic reaction coordinate[56,57] (IRC) calculations in acetonitrile solution (COSMO-ADC(2)/SVP) are pursued on the S_1 potential energy surface (PES) starting from the Franck-Condon point (ground state equilibrium geometry). The results of COSMO-ADC(2)/def2-TZVPP calculations along the IRC path are shown in Fig. 5. After an initial phase, the complex reaches a region where the S_1 PES is very flat and might, if explicit solvent molecules would be included, have shallow minima. Thus, in solution, where the excess vibrational energy is dissipated to the solvent, the complex should stay for some time in this region before it eventually reaches on the S_1 PES the mimimum structure S_1-eq.

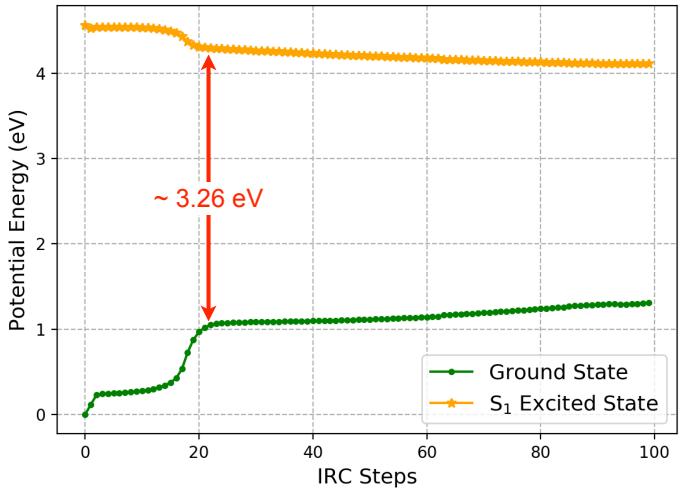


Fig. 5 BrBzImOTf: Ground- and excited-state energy obtained with COSMO-ADC(2)/def2-TZVPP (post-SCF reaction-field scheme) along the IRC path for the relaxation of on the S_1 PES starting from the S_{0-eq} (Franck-Condon point). Note that the time along the IRC path has no direct physical meaning.

Fig. 6a shows in the first phase of the deexcitation process a fast bending of Br–C bond out of the benzimidazolium ring plane together with a concurrent elongation of the Br–C bond (cmp. Fig. 6b). The out-of-plane angle for the C–S connection line, which is used to track the motion of the OTf^- counterion, follows in this first phase closely the C–Br out-of-plane angle. However, in the second phase, where the S_1 PES becomes very flat, the out-of-plane angle of the C–S connection line decreases slightly while the C–Br bond continues to bend and stretch further. For this region the calculations predict fluorescence at 3.26 eV or 380 nm. In the calculations, we do not observe a complete dissociation of the C–Br bond. We note, however, that in ADC(2) calculations the ground state is described with MP2 which is not suited to describe homolytic bond cleavages. As described above, an unconstrained geometry optimization on the S_1 PES starting from the Franck-Condon point ends at the S_1-eq geometry shown in Fig. 3e with the structure of an anion-π complex with an out-of-plane tilted C–Br bond.

In summary, the calculations indicate that the formation of a halogen bond with OTf^- in acetonitrile solution does not change

Published on 09 March 2021. Downloaded by Ruhr Universitat Bochum on 3/9/2021 10:47:03 AM.
Physical Chemistry Chemical Physics Accepted Manuscript

View Article Online
DOI: 10.1039/D1CP00009H

Published on 09 March 2021. Downloaded by Ruhr Universitat Bochum on 3/9/2021 10:47:03 AM.

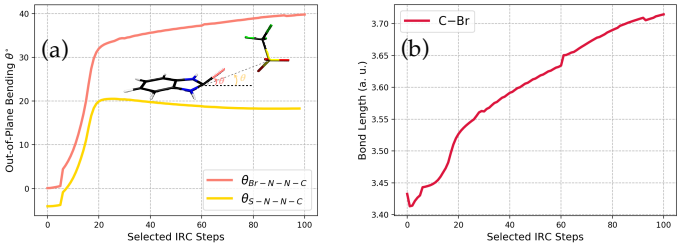


Fig. 6 BrBzImOTf: Evaluation of (a) the out-of-plane bending of the C–Br bond (salmon) and the SO_3 moiety of the OTf^- (gold) with respect to the planar benzimidazolium and (b) the C–Br bond length along the IRC path calculated at COSMO-ADC(2)/def2-TZVPP level at the lowest electronically excited state S_1.

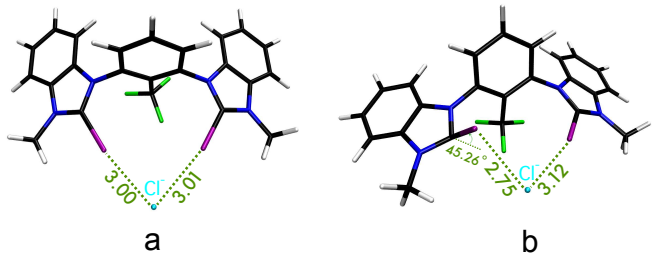


Fig. 7 Optimized geometries of $BIBzImCl^+$ in (**a**) the ground state S_0-eq with XB interaction at the COSMO-MP2/def2-TZVPP(PTE) level and (**b**) the first excited state S_1-eq at the COSMO-RI-ADC(2)/def2-TZVPP(post-SCF) level in acetonitrile solution.

the energy of the bright $\pi\pi^*$ transition significantly. Furthermore, if regarded separately, the extension of the π-system may in principle increase the excited-state lifetime of the XB IBzImOTf complex relative to the IImOTf and enhance the fluorescence emission. The calculations predict that the XB interaction red shifts the fluorescence signal, particularly for the BrBzImOTf, if the emission happens close to the S_1-eq geometry. In the ground state, the binding energy of OTf^- to the $IBzIm^+$ cation is 7.4 kcal·mol^{-1}. This energy increases in the excited state to 14.4 kcal·mol^{-1} due to the $n\sigma^*$ character of the excited state at the S_1-eq geometry which is stabilized by the presence of the counterion. One can altogether conclude that monodentate 2-iodoimidazolium cations dissolved in acetonitrile are only weak XB donors that should not exhibit any significant changes in their absorption spectra attributable to the XB interaction, while the emission energy for the optimized S_1-eq geometry strongly depends on the XB, thus foreshadowing that the fluorescence characteristics might be dependent on the XB as well.

6 Bis(2-Iodo-benzimidazolium)·Cl

The bis(2-iodobenzimidazolium) dication ($bIBzIm^{2+}$) can potentially act as a bidentate Lewis acid. The rotation of the halobenzimidazolium moieties around the C–N axis which connects these groups to the benzene core are sterically inhibited by the trifluoromethyl group in the 2-position of the 1,3-disubstituted benzene ring.[17] The bidentate structure of the $bIBzIm^{2+}$ cation prompted us to study this compound as a halogen-bond donor in an XB complex with a chloride counterion (Cl^-), Fig. 7a. The binding energy of Cl^- to the $bIBzIm^{2+}$ dication in acetonitrile solution is $\approx$ 18.6 kcal·mol^{-1} in the ground state and increases in S_1 at the S_1-eq structure to 28.7 kcal·mol^{-1}. These binding energies are much higher than the corresponding values for the monodentate IIm^+ and $IBzIm^+$ cations with the OTf^- counterion.

The UV-Vis absorption spectra for the XB complex were calculated in acetonitrile solution and in vacuum and the results for the excitation energies and oscillator strengths for the lowest five electronic excited states are shown in Fig. 8 and Table S11 of the SI. In solution the excitation energies, intensities and also the characters of the excited states change relative to the vacuum. As shown in Fig. 8, in solution the S_1 and S_2 states are nearly degenerate at excitation energies of 4.53 eV and 4.59 eV with S_2 as the brightest state. These two excitations are comprised of plus and minus combinations of $\pi\pi^*$ transitions mainly localized on the 2-iodobenzimidazolium moieties with a partial CT from iodine to the π^* orbitals of the π-conjugated benzimidazolium rings. The NTOs given for the excited states of the XB complex in Fig. 8 clearly show that the negative charge on the Cl^- is stabilized by the polar solvent which results in negligible contributions from the orbitals at the Cl^- counterion to the NTOs for the lowest five states. The third and forth states (S_3 and S_4) are located at, respectively, 4.90 eV and 4.93 eV of the spectrum with S_3 carrying a significant oscillator strength of 0.35. Similar as for S_1 and S_2, these two states are comprised of symmetric and antisymmetric linear combinations of local $\pi\pi^*$ transitions on the two iodobenzimidazolium moieties. The first transition localized on the central benzene linker appears as S_5 at 4.95 eV. Because of its small oscillator strength this state does not contribute to the UV absorption spectrum of the XB complex.

The four lowest electronic transitions of the $bIBzIm^{2+}$ dication without counterion have similar characters and oscillator strengths as for the XB complex (cmp. Table 3 and Table S13 of the SI). The XB interaction does not effect the energies of the S_1 and S_2 states compared to the dication, while it blue shifts the energies of S_3 and S_4 by $\approx$ 0.1 eV. The S_5 state of diaction is a $\pi\sigma^*$ transition from the π orbitals of the iodoimidazolium moieties to the σ^* orbital of the C–I bonds and is a dark state.

Table 3 Vertical excitation energies ΔE (eV) and oscillator strengths f of the XB $bIBzImCl^+$ complex and $bIBzIm^{2+}$ dication in acetonitrile at the COSMO-ADC(2)/def2-TZVPP(post-SCF) level.

	$bIBzImCl^+$			$bIBzIm^{2+}$		
State	Type	ΔE	f	Type	ΔE	f
1	$1\pi\pi^*$	4.53	0.197	$1\pi\pi^*$	4.54	0.120
2	$2\pi\pi^*$	4.59	0.616	$2\pi\pi^*$	4.58	0.605
3	$3\pi\pi^*$	4.90	0.353	$3\pi\pi^*$	4.81	0.302
4	$4\pi\pi^*$	4.93	0.067	$4\pi\pi^*$	4.83	0.059
5	$5\pi\pi^*$	4.95	0.010	$\pi\sigma^*$	5.00	0.004

The results for the vertical excitation of the XB complex in vacuum reveal that the lowest five electronic states have CT character. They are transitions mainly from non-bonding orbitals of Cl^- to the imidazolium moieties and the phenyl ring. The two close-lying S_1 and S_2 states in vacuum appear at $\approx$ 4.30 eV and carry oscillator strengths of $\approx$ 0.2. The S_3 state at 4.45 eV is a CT tran-

Physical Chemistry Chemical Physics Accepted Manuscript

View Article Online
DOI: 10.1039/D1CP00009H

Published on 09 March 2021. Downloaded by Ruhr Universitat Bochum on 3/9/2021 10:47:03 AM.

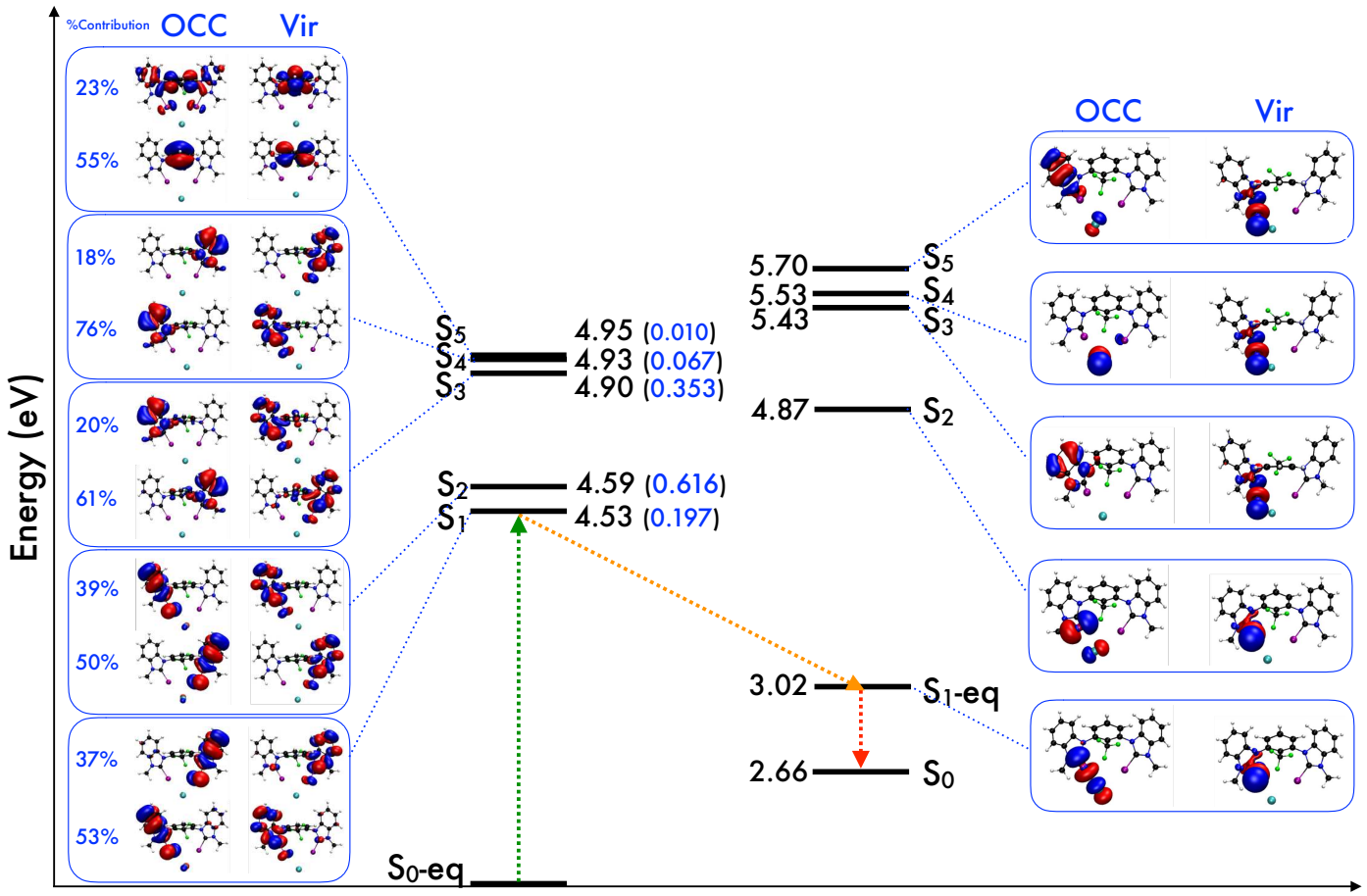


Fig. 8 bIBzImCl$^+$: Natural transition orbitals, vertical excitation energies (eV) (green arrow) and oscillator strengths (in blue) at the Franck-Condon geometry of the XB complex. A geometry optimization on the S_1 potential energy surface leads to S_1-eq (orange arrow). The emission energy (eV) at the S_1-eq structure to S_0 is indicated by a red arrow. All excited-state calculations are at the COSMO-RI-ADC(2)/def2-TZVPP(post-SCF) level in acetonitrile solution. The ground-state geometry of S_0-eq was optimized at the COSMO-MP2/def2-TZVPP(PTE) level in acetonitrile.

Physical Chemistry Chemical Physics Accepted Manuscript

View Article Online
DOI: 10.1039/D1CP00009H

Published on 09 March 2021. Downloaded by Ruhr Universitat Bochum on 3/9/2021 10:47:03 AM.

sition from non-bonding orbitals at chloride and iodine into the central benzene linker. The S_4 and S_5 states at 4.48 and 4.54 eV are, respectively, symmetric and antisymmetric combinations of $n\pi^*$ CT transitions from Cl^- to the imidazolium moieties.

Going back to the results in solution, as pointed out above, S_1 and S_2 are at the almost C_S-symmetric ground state structure nearly degenerate mixtures of the lowest local excitations in the benzimidazolium groups. The relaxation after photoexcitation from the Franck-Condon point towards the minima on the excited state potential energy surface breaks the near C_S symmetry and leads to a localization of S_1 on one and S_2 on the other benzimidazolium group and should end in two symmetry-equivalent minima on the excited-state potential. The result for the equilibrium structure reached after relaxation from the Franck-Condon point in the S_1 state, S_1-eq, in acetonitrile solution is given in Fig. 7b. The relaxation slightly twists the complex and leads after localization of the excitation on one side of the complex to similar structural changes in the corresponding iodoimidazolium group as observed in the previous sections with an out-of-plane bending angle of the C–I bond by $\approx 45°$ and a lengthening of the C–I bond by 0.36 Å. The NTOs for the S_1 transition at the S_1-eq geometry shown in Fig. 8 indicate that an electron is excited from an anti-bonding orbital between iodine and chloride to the σ^* orbital of the C–I bond. This explains the elongation of the C–I bond length compared to the ground state geometry, Fig. 7a, from 2.05 to 2.41 Å, while the other C–I bond length remains almost unchanged, and at the some time, the shortening of the I–Cl distance by ≈ 0.25 Å.

For the $bIBzIm^{2+}$ dication without the XB partner, the relaxation from the Franck-Condon point to the associated S_1-eq geometry is accompanied with an out-of-plane bending by $\approx 43°$ and an elongation of the C–I bond for one of the imidazolium groups. However, in this case the C–I bond elongation is with 0.18 Å significantly smaller than in the XB complex. The NTOs of the S_1 state at the S_1-eq structure of the dication in Fig. 9 show a CT from π^* orbitals of one of the iodoimidazolium fragments to the σ^* orbital of the C–I bond. The emission energy at this structure from S_1 to S_0 is with 2.30 eV almost 2 eV larger than for the XB complex in Fig. 8, where the S_1-eq structure is stabilized by the formation of a partial covalent I–Cl bond. For both the XB complex and the dication, after deexcitation from S_1-eq to S_0 the structures relax back to the original ground state minimum S_0-eq.

Thus, for the $bIBzImCl^+$ complex, after excitation into S_1 the XB interaction stays intact and is even strengthened during the relaxation to the S_1-eq structure. The strong stabilization of S_1-eq should have a large influence on the fluorescence spectrum. At the same time, for the dication without XB partner our calculations predict a larger fluorescence emission energy.

7 Spectroscopic Results

For the experimental studies, we restrict the discussion to five benzimidazolium ($BzIm^+$) compounds for which transiently as well as spectrally resolved fluorescence spectroscopy is performed. Since the compounds are cations, we look for signatures of ions pairing with counter-anions reflected in the UV-Vis absorption or emission characteristics, an approach which is mostly sensitive to contact-ion pairs[58] like they are found in the computations.

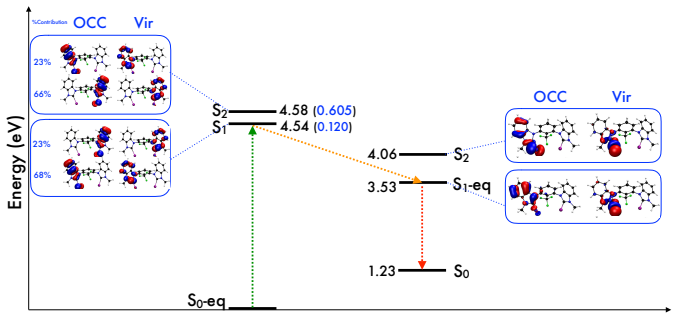


Fig. 9 $bIBzIm^{2+}$: Natural transition orbitals, vertical excitation energies (eV) (green arrow) and oscillator strengths (in blue) at the Franck-Condon geometry. A geometry optimization on the S_1 potential energy surface leads to S_1-eq (orange arrow). The emission energy (eV) at S_1-eq to S_0 is indicated by a red arrow. All excited-state calculations are at the COSMO-RI-ADC(2)/def2-TZVPP(post-SCF) level in acetonitrile solution. The ground-state geometry of S_0-eq was optimized at the COSMO-MP2/def2-TZVPP(PTE) level in acetonitrile.

Besides the properties of the solvent, the choice of counter-anion can play a decisive role with regard to the photophysics of cationic dyes in solution.[59–63] Small anions can interact with the π system of the cationic compound, which may get polarized by the anion, leading to variations in the extinction coefficient ε and/or to spectral shifts; bulky anions lead to larger interion distances and hence the spectral features of the cation should be much less affected.[62,63]

As two anions with very different ion pairing characteristics, we choose OTf^- and $[BAr_4^F]^-$ (for an insightful juxtaposition of these two anions, see Section 6.2 in Ref. 64). The latter is rather large and only modestly capable to form ion pairs[64,65], and due to the high symmetry there is no pronounced localization of charge density on the anion's periphery.[63] OTf^- is much smaller (with a hydrodynamic radius roughly half that of $[BAr_4^F]^-$, depending on the solvent) and the negative charge is localized on the molecular moiety with the oxygen atoms.[64]

The absorption spectra of the studied compounds in acetonitrile solution are displayed in Fig. 10a. They only absorb in the UV spectral range, with the halogenated $BzIm^+$ species exhibiting a red-shift compared to the hydrogenated or methylated ones. Whereas the OTf^- does not absorb in this spectral region, $[BAr_4^F]^-$ has an absorption, as is evidenced by the curve for $NaBAr_4^F$ solutions (blue line in Fig. 10a). For cyanine dyes in acetonitrile,[63] it has been observed that the counter-anion leads to changes of ε while the absorption peak position is unaltered. A similar situation is found for our systems, as the absorption spectrum of $IBzImBAr_4^F$ (red line in Fig. 10a) can be almost perfectly reproduced by a linear combination (dotted line in Fig. 10a) of the spectra of IBzImOTf (black line in Fig. 10a) and of $NaBAr_4^F$ (blue line in Fig. 10a).

The four different $BzIm^+$ cations all fluoresce after photoexcitation at 266 nm, the corresponding emission spectra are shown in Fig. 10b. The $[BAr_4^F]^-$ anion also exhibits a faint fluorescence signal (blue line in Fig. 10b). The fluorescence intensity of HBzI-

Physical Chemistry Chemical Physics Accepted Manuscript

View Article Online
DOI: 10.1039/D1CP00009H

Published on 09 March 2021. Downloaded by Ruhr Universitat Bochum on 3/9/2021 10:47:03 AM.

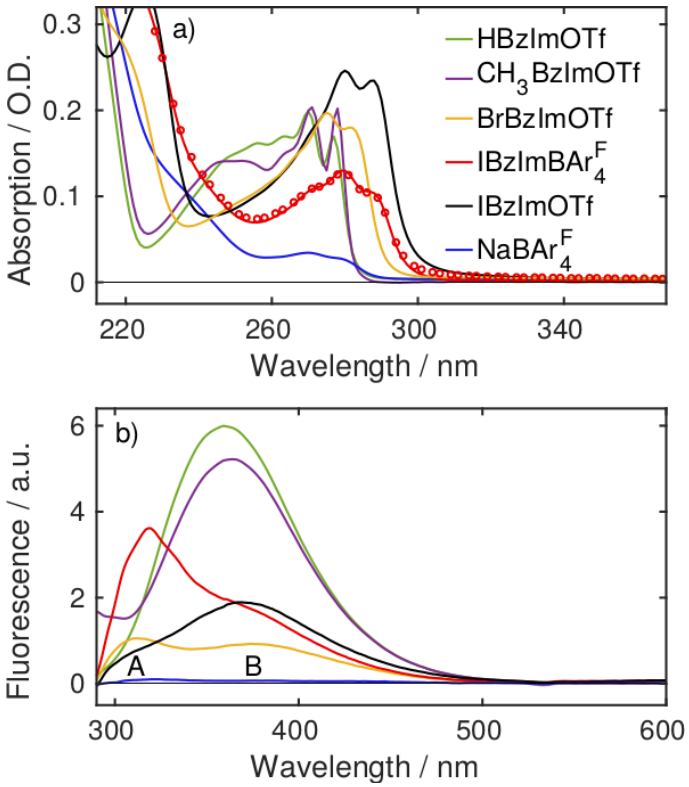


Fig. 10 (**a**) Absorption and (**b**) fluorescence spectra after 266 nm excitation of the studied compounds in actonitrile (390 μM) of the six samples HBzImOTf (green), CH_3BzImOTf (purple), BrBzImOTf (orange), IBzImBAr$_4^F$ (red), IBzImOTf (black), and NaBAr$_4^F$ (blue). The dotted line in (**a**) is a linear combination of the spectra of IBzImOTf and of NaBAr$_4^F$. The fluorescence intensity of HBzImOTf and CH_3BzImOTf was demagnified by a factor of 100.

mOTf (green in Fig. 10b) and CH_3BzImOTf (purple in Fig. 10b) was demagnified by 10^{-2}, because these compounds show a much stronger emission signal.

When $BzIm^+$ is halogenated, spin-orbit coupling may be increased, a phenomenon known as the internal heavy atom effect (IHAE)[66–72]. This effect facilitates nonradiative S_1 deactivation mostly caused by enhanced intersystem crossing $S_1 \rightarrow T_1$, thus lowering the fluorescence quantum yield and shortening the S_1 lifetime. Furthermore, the significantly lowered fluorescence quantum yield in case of the halogenated compounds may be a consequence of an ultrafast transition from the excited $\pi\pi^*$ state to a non-fluorescent $\pi\sigma^*$ state, originating from out-of-plane motion of the bond involving the halogen atom[73–79], as also reflected in our simulations. As disclosed by Domcke, Sobolewski, and colleagues[73–76] for related compounds such as phenol and chlorobenzene, the $\pi\pi^*$ state reached upon excitation exhibits a conical intersection with the repulsive $\pi\sigma^*$ state, with the energetic minimum of the $\pi\pi^*$ state being lower in energy so that a barrier has to be overcome, e.g. in a predissociative step (we conjecture that especially in solution this might not occur for all molecules). Once populated, the $\pi\sigma^*$ state may lead to fission of the carbon–halogen bond or to internal conversion back to the ground state, the latter being facilitated by a further conical intersection of the $\pi\sigma^*$ state with the ground state.[73] Remarkably, it was shown that complexation involving a hydrogen bond (and thus maybe also an XB) strongly impacts the $\pi\sigma^*$ state and may remove the latter conical intersection,[74] thereby presumably modifying the relative branching of the competing processes fluorescence, internal conversion, and bond fission. In this regard, halogens are known to be good photoleaving groups, so that the bond between the halogen and the carbon atom may be cleaved upon photoexcitation, i.e. also holding the molecule from fluorescing, often followed by recombination to the initial molecule.[81] Therefore, transient signals from halogenated species in solution have been reported to decay faster and be lower in amplitude[71] than unhalogenated ones. Although the fluorescence signals observed here for the halogenated $BzIm^+$ species are much weaker compared to the hydrogenated or methylated analogues because of these phenomena, ion pairing contributions are educible, as is outlined in the following.

In contrast to the absorption, the emission spectra of IBzImBAr$_4^F$ is not just a linear combination of the ones for IBzImOTf and NaBAr$_4^F$. Furthermore, the long-wavelength edge reveals that the fluorescence has a slight bathochromic shift for IBzImOTf compared to IBzImBAr$_4^F$. Since the bulky, distant [BAr$_4^F$]$^-$ is expected to have a much smaller effect on the excited state of $IBzIm^+$ than OTf^-, this shift may be indicative of ion pairing, as deduced for other dyes in acetonitrile.[63] The fluorescence signal of BrBzImOTf (orange line in Fig. 10b) is comprised of two parts, one at ≈315 nm (labeled peak A) and a second one at ≈380 nm (labeled B), respectively. For IBzImBAr$_4^F$ (red line in Fig. 10b), peak A is the dominant contribution, which however is virtually absent for IBzImOTf (black curve in Fig. 10b) and is also not found for HBzImOTf and CH_3BzImOTf (green and purple line in 10b).

Stationary fluorescence spectra already give an indication which features might originate from ion pairing. For additional insight, we further study the emission characteristics in a time-resolved manner. Transient fluorescence spectra for the five $BzIm^+$ samples are shown in the left column of Fig. 11. The fluorescence decays on a timescale of several nanoseconds, but for the halogenated species, additional dynamics and spectral shifts are observed. This is substantiated by the decay-associated spectra (DAS) given in the right column of Fig. 11.

The fluorescence decays of HBzImOTf (Fig. 11a) and CH_3BzImOTf (Fig. 11b) show absolutely no spectral shifts with time and can each be described very well by a monoexponential model, leading to one almost Gaussian-shaped DAS for each compound and corresponding excited-state lifetimes of 7.4 ns and 7.1 ns, respectively. Whereas an interaction of OTf^- with the π-system of the $BzIm^+$ moiety might occur, an XB is impossible due to the lack of a halogen atom. We therefore ascribe the dynamics on a timescale of ≈7 ns to effects not related to an XB and not comprising large geometrical reorganization of the cation in the excited state.

In contrast to the strong fluorophores HBzImOTf and CH_3BzImOTf which show emission decaying with one characteristic lifetime, the other three halogenated samples require a non-monoexponential decay model (SI, Fig. S1). In particular

Physical Chemistry Chemical Physics Accepted Manuscript

View Article Online
DOI: 10.1039/D1CP00009H

Published on 09 March 2021. Downloaded by Ruhr Universitat Bochum on 3/9/2021 10:47:03 AM.

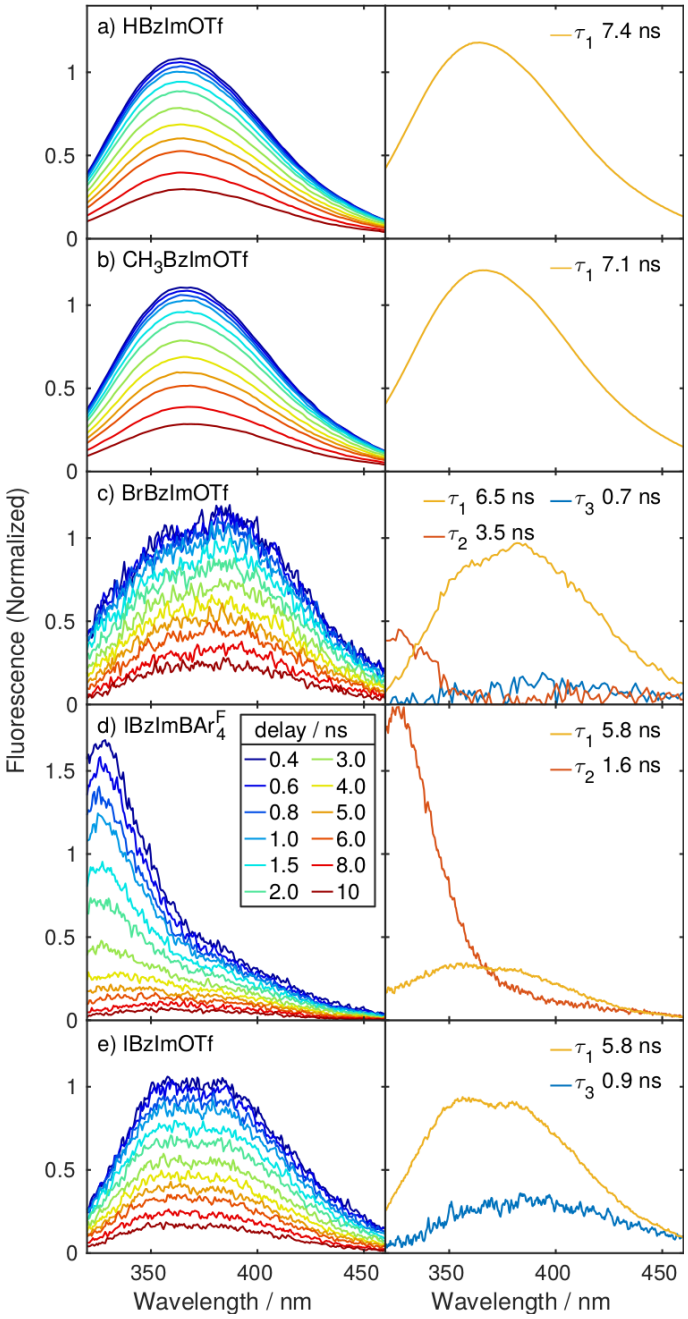


Fig. 11 Transient fluorescence spectra (left) and decay-associated spectra (right) for the five $BzIm^+$ compounds in acetonitrile solution (390 μM) after 266 nm excitation. For comparability, each data set is normalized to the signal at an emission wavelength 350 nm and at a delay of 0.4 ns. Note that there is a lower sensitivity of the transient fluorescence setup for shorter wavelengths, so that the actual shape of the spectra towards the UV is slightly contorted.

for BrBzImOTf (Fig. 11c), three DAS are required to describe the data. Again, there is a strong contribution on a 7 ns timescale (τ_1=6.5 ns) with a DAS similar to a Gaussian which we interpret analogously as for the non-halogenated molecules. Measurements of stationary absorption spectra after hours of illumination have shown that the bromine is not irreversibly photolyzed off (*vide infra*), therefore fluorescence contributions from dehalogenated molecules are discarded.

Furthermore, the determined order $\tau_1^I < \tau_1^{Br} < \tau_1^{CH_3} < \tau_1^H$ for the different substituents is in accord with an IHAE, thus indicating that the τ_1 contribution originates from the intact $BzIm^+$ species. Besides τ_1, there is also more rapid fluorescence dynamics with a decay constant of τ_2=3.5 ns on the blue edge of the spectrum with a peak at 320 nm and even faster contribution of τ_3=0.7 ns with its maximum around 400 nm. The Gaussian-shaped τ_1 DAS contributes most to the steady-state fluorescence spectra (orange line in Fig. 10b), nonetheless the appearance of peaks A and B, as observed in the steady-state fluorescence, is retrieved again by τ_2 and τ_3, respectively.

The iodated $BzIm^+$ compounds $IBzImBAr_4^F$ (Fig. 11d) and IBzImOTf (Fig. 11e) exhibit only one additional second fluorescence decay besides the 7 ns component. However, it is only located in the spectral region of peak A for $IBzImBAr_4^F$ (τ_2=1.6 ns), whereas it comprises the region of peak B in the case of IBzImOTf (τ_3=0.9 ns). A possibly interfering signal of the very weakly emitting counterion $[BAr_4^F]^-$ (compare $NaBAr_4^F$ in Fig. 10b) can be excluded by the corresponding impact study (SI, Fig. S2).

The τ_2 and τ_3 dynamics (red and blue DASs in Fig. 11) might be associated with subensembles of molecules that perform an additional deactivating motion which effectively quenches the excited state. From the results of the calculations, we infer that this motion might be the out-of-plane bending of the bond between the halogen atom and the carbon it is covalently bound to, a motion possible both with and without an OTf^- counterion, but to a different extent (compare the computational result for IBzImOTf and BrBzImOTf). For the bulky counter-anion $[BAr_4^F]^-$, for which ion pairing should be negligible, peak B is not observed (Fig. 11d). Therefore, we conclude that peak A, i.e. the fast fluorescence below 350 nm (τ_2), is associated with this motion.

The calculations have also shown that XB formation with OTf^- is possible, and that the fluorescence is strongly red-shifted in this case. The IRC calculations for BrBzImOTf showed that after a short initial relaxation phase, where the C–Br bond bends out of the molecular plane, the contact ion pair reaches a region where the S_1 surface is very shallow. The vertical fluorescence energy is for this region computed as $\approx$ 3.26 eV or $\approx$ 380 nm in a good agreement with the position of peak B. Hence, we assign peak B to the fluorescence of molecules that undergo the C–I out-of-plane bending motion when an XB is present (τ_3). Thus, with the large $[BAr_4^F]^-$, mostly peak A is observed, whereas with the small OTf^-, peak B prevails. This suggests that a certain amount of molecules is ion-paired in the acetonitrilic solution of IBzImOTf.

Generally, the ability to form an XB is stronger for iodine than it is for bromine[82], therefore the amount of X-bonded pairs should be less pronounced in the case of BrBzImOTf than it is for IBzImOTf. This is corroborated by the red (τ_2) and blue (τ_3) DAS in Fig. 11c which comprise both peaks A and B. Along the lines of our interpretation, this means that our experiments with BrBzImOTf monitor the C-Br out-of-plane bending motion in $BrBzIm^+$ cations without (peak A) or with (peak B) an X-bonded OTf^-, respectively.

Physical Chemistry Chemical Physics Accepted Manuscript

View Article Online
DOI: 10.1039/D1CP00009H

Published on 09 March 2021. Downloaded by Ruhr Universitat Bochum on 3/9/2021 10:47:03 AM.

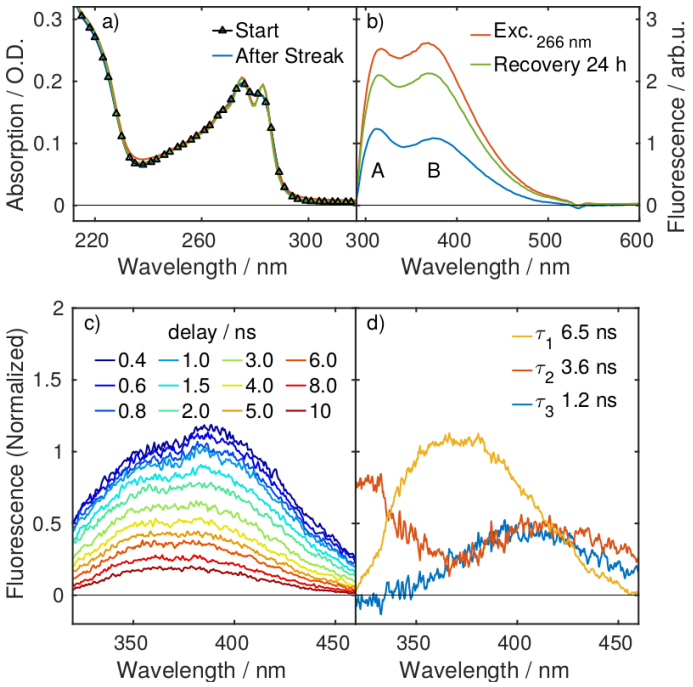


Fig. 12 (**a**) Absorption and (**b**) fluorescence spectra after 266 nm excitation of BrBzImOTf in acetonitrile solution (390 μM) before (black line and triangles) and right after the first transient measurement (blue line), after distinct UV irradiation (red) and after additional 24 h of recovery (green). Transient fluorescence spectra (**c**) and the decay-associated spectra (**d**) after distinct UV irradiation (excited at 266 nm). Note that there is a lower sensitivity of the transient fluorescence setup for shorter wavelengths, so that the actual shape of the spectra towards the UV is slightly contorted [so that peak A is less pronounced in (c) than in (b)].

Since absorption spectra indicate no irreversible photolysis of the halogen atom for the BrBzImOTf sample (in contrast to IBzImOTf where irreversible photocleavage of iodine is observable), an investigation in the complex formation and equilibrium distribution among the different possible ion-pair complexes is pursued by extended UV illumination. The corresponding results are shown in Fig. 12 starting with the stationary absorption (a) and fluorescence (b) measurements. No change is observable for the absorption spectra obtained before (black line in Fig. 12a) and after (blue line) the transient fluorescence measurements of Fig. 11. However, after 2 hours of UV irradiating a 100 μL sample volume with the excitation laser (266 nm), the characteristic double peak in the absorption spectrum sharpens and the corresponding fluorescence intensifies (red lines in Fig. 12a and b). Furthermore, the proportion of peaks A and B shifts towards B. Within 24 further hours in the dark, the sample begins to recover, as is most evident in the fluorescence spectrum (green line in Fig. 12b). With the irradiation turned back on, the fluorescence increases again, counteracting the recovery.

The transient fluorescence behavior of the BrBzImOTf sample after 2 hours of UV irradiation (corresponding to the red lines in Fig. 12a and b) is displayed in Fig. 12c, the respective DASs in Fig. 12d. In comparison to the initial measurement shown in Fig. 11c, the τ_1 DAS assigned to the excited state without ion-pairing or out-of-plane bending stays unchanged. By contrast, the contributions of the two faster decays get more intense. Beyond that, an additional signal arises, with a decay behavior associated with τ_2 but with a spectral shape similar to the DAS of τ_3.

In view of the calculations (*vide supra*) the observed differences might originate from a changed distribution of the different ion-pair complexes. The calculations have shown that after exciting the halogen-bonded complex, the counterion OTf^- moves out of plane and leads to an ion pair held together by anion-π interaction. The theoretical COSMO-MP2 investigation has also shown that this ion pair is more stable than the one with an XB, thus if re-excited it might emit bathochromically shifted and give rise to the additional signal. From its spectral position, we further conjecture that the particular re-excited $BrBzIm^+$ may perform the same out-of-plane bending motion as the previously assigned XB complex (peak B). In contrast to the former XB complex, the resulting emission decay from S_1-eq is slowed down and on a time scale similar to the dynamics of the lone $BrBzIm^+$ cation (peak A).

The proportion between the τ_1 DAS and the deactivation channels putatively involving out-of-plane bending motion of the halogen (i.e., the τ_2 and τ_3 DASs) shifts towards the latter under UV irradiation. This might imply that by persisting illumination of the sample, the newly formed anion-π complex is accumulated (and can slowly relax back in the dark, as seen in Fig. 12b), which in turn leads to a relative decrease of the signals assigned to rigid $BrBzIm^+$ not interacting with an OTf^- (τ_1 DAS). The fastest decaying signal associated with the τ_3 DAS also shows this relative increase in Fig. 12d compared to Fig. 11c, possibly suggesting that shifting the equilibrium towards ion pairs also increases the relative share of halogen-bonded ones. However, since τ_3 is 0.7 ns before and 1.2 ns after the illumination, it is also possible that the blue DAS is also linked to the newly formed species. A further hint in this direction might be the line sharpening in the absorption spectrum (Fig. 12a) which could indicate that the accumulation of the anion-π complex is connected with less proximity broadening in the UV spectrum than maybe an ion pair with an XB is. Overall, the spectroscopic studies substantiate that ion pairing occurs and also provide reason that signatures of XB formation are contained in the (time-resolved) spectra.

8 Conclusion

In this joint theoretical and experimental study, ion pairing of halogenated imidazolium compounds with counter-anions via a halogen bond was investigated. In the theoretical studies, we used the correlated wavefunction-based method ADC(2) in combination with the COSMO solvation model to unveil effects of the halogen-bond interaction on the excited states of iodo- and bromo-imidazolium compounds. In particular, we studied the excited-state minima reached by relaxation on the S_1 PES, the IRC pathway for the relaxation, and the emission energies to understand the influence of the halogen-bond interaction on the fluorescence properties of these compounds. To this end, we studied the five lowest excited states of the XB complexes IImOTf, IBzImOTf, BrBzImOTf, and $bIBzImCl^+$ in acetonitrile solution and analyzed the corresponding NTOs. The inclusion of a solvent model proves to be essential because the results in vacuum predict completely different spectra due to a strong overestimation

Physical Chemistry Chemical Physics Accepted Manuscript

View Article Online
DOI: 10.1039/D1CP00009H

Published on 09 March 2021. Downloaded by Ruhr Universitat Bochum on 3/9/2021 10:47:03 AM.

of the interaction between the ions without screening dielectric environment.

For IImOTf, IBzImOTf and BrBzImOTf on the S_1 PES the calculations predict relaxation pathways which after deexcitation lead to other minima on the ground-state PES with anion-π interactions between the counterion and one face side of the imidazolium ring. As an excited-state pathway, an out-of-plane bending of the C-I bond is identified, so that the two face sides are not identical and the anion-π interaction occurs preferentially on the side to where the C–I bond has bent.

For the bidentate XB complex, the relaxation on the S_0 PES after deexcitation at the excited-state equilibrium structure S_1-eq brings the molecule back to the original ground-state XB structure S_0-eq. Hence, the bidendate XB complex may not only have a fluorescence that is red shifted relative to the dication without counterion, but may also stay intact, i.e. with the XB preserved, after photoexcitation and subsequent return to the ground state.

For all four cations, examination of the influence of the XB on the excited-state properties in solution by excluding the counterion from the calculations gave excited states that are mostly similar to those for the corresponding XB complexes.

In spectroscopic studies comprising stationary absorption and emission studies as well as time-resolved fluorescence, the compound IBzImOTf and BrBzImOTf from the calculations and the related HBzImOTf, CH_3BzImOTf, and IBzImBAr$^F_4$ were investigated in acetonitrile solution. Whereas the fluorescence dynamics are monoexponential with a decay time of about 7 ns in non-halogenated systems, spectral signatures associated with a faster timescale could be identified for the halogenated ones which exhibit an emission which is spectrally different but overall two orders of magnitude lower in amplitude than for the non-halogenated systems. This additional signal found for IBzImBAr$^F_4$ is blue-shifted, while the one for IBzImOTf is red-shifted relative to the spectrum of the 7 ns dynamics. We attribute the latter contribution to the C–I out-of-plane bending in the contact ion pair observed in the calculations and ascribe the differences to the presence of an XB in the case of IBzImOTf or to the absence of an XB in the case of IBzImBAr$^F_4$. The significantly lower fluorescence quantum yield for the halogenated species might originate from a competing transition from the $\pi\pi^*$ to the $\pi\sigma^*$ state which is non-emissive; hence, it is not directly traceable by time-resolved fluorescence but will be addressed in future ultrafast transient absorption studies.

Experiments with BrBzImOTf, with the weaker XB donor Br compared to I, disclosed that both peaks are observed, which we interpret as an ensemble effect with both molecules with and without an XB existent in the solution. After hours of UV illumination, the stationary spectra as well as the time-resolved fluorescence changes so that the possibility of more than one ion-pair species is considered, in accord with results from theory.

These joint investigations illustrate that halogenated imidazolium compounds in acetonitrile may act as XB donors, an interaction which is reflected both in calculated transition energies and time-resolved fluorescence data.

Conflicts of interest

There are no conflicts to declare

Acknowledgements

We acknowledge financial support by the Deutsche Forschungsgemeinschaft through project Ha 2588/8-1. Funded by the Deutsche Forschungsgemeinschaft (DFG, German Research Foundation) under Germany's Excellence Strategy - EXC 2033 — 390677874 — RESOLV. PN and BG further thank the DFG (GRK 2620 Ion Pair Effects) for intellectual support.

Notes and references

1 R. Gajda, A. Katrusiak and J. Crassous, *Cryst. Eng. Comm.*, 2009, **11**, 2668–26776.
2 H. L. Nguyen, P. N. Horton, M. B. Hursthouse, A. C. Legon and D. W. Bruce, *J. Am. Chem. Soc.*, 2004, **126**, 16–17.
3 K. E. Riley and P. Hobza, *J. Chem. Theory Comput.*, 2008, **4**, 232–242.
4 S. Kozuch and J. M. L. Martin, *J. Chem. Theory Comput.*, 2013, **9**, 1918–1931.
5 L. P. Wolters, P. Schyman, M. J. Paven, W. L. Jorgensen, T. M. Bickelhaupt and S. Kozuch, *WIREs Comput. Mol. Sci.*, 2014, **4**, 523–540.
6 S. Lindblad, K. Mehmeti, A. X. Veiga, B. Nekoueishahraki, J. Gräfenstein and M. Erdélyi, *J. Am. Chem. Soc.*, 2018, **140**, 13503–13513.
7 Y. Lu, H. Li, X. Zhu, H. Liu and W. Zhu, *Int. J. Quantum Chem.*, 2012, **112**, 1421–1430.
8 S. H. Jungbauer, S. Schindler, F. Kniep, S. M. Walter, L. Rout and S. M. Huber, *Synlett.*, 2013, **24**, 2624–2628.
9 F. Kniep, L. Rout, S. M. Walter, H. K. V. Bensch, S. H. Jungbauer, E. Hertweck and S. M. Huber, *Chem. Commun.*, 2012, **48**, 9299–9301.
10 R. Tepper, B. Schulze, M. Jäger, C. Friebe, D. H. Scharf, H. Görls and U. S. Schubert, *J. Org. Chem.*, 2015, **80**, 3139–3150.
11 G. Cavallo, P. Metrangolo, R. Milani, T. Pilati, A. Priimagi, G. Resnati and G. Terraneo, *Chem. Rev.*, 2016, **116**, 2478–2601.
12 A. Siiskonen and A. Priimagi, *J. Mol. Model*, 2017, **23**, 50.
13 L. N. Anderson, F. W. Aquino, A. E. Raeber, X. Chen and B. M. Wong, *J. Chem. Theory Comput.*, 2018, **14**, 180–190.
14 T. M. Beale, M. G. Chudzinski, M. G. Sarwar and M. S. Taylor, *Chem. Soc. Rev.*, 2013, **42**, 1667–1680.
15 L. C. Gilday, S. W. Robinson, T. A. Barendt, M. J. Langton, B. R. Mullaney and P. D. Beer, *Chem. Rev.*, 2015, **115**, 7118–7195.
16 Y. Lu, H. Li, X. Zhu, W. Zhu and H. Liu, *J. Phys. Chem. A*, 2011, **115**, 4467–4475.
17 S. H. Jungbauer and S. M. Huber, *J. Am. Chem. Soc.*, 2015, **137**, 12110–12120.
18 S. H. Jungbauer, S. M. Walter, S. Schindler, L. Rout, F. Kniep and S. M. Huber, *Chem. Commun.*, 2014, **50**, 6281–6284.

Physical Chemistry Chemical Physics Accepted Manuscript

View Article Online
DOI: 10.1039/D1CP00009H

Published on 09 March 2021. Downloaded by Ruhr Universitat Bochum on 3/9/2021 10:47:03 AM.

19 Y. Takeda, D. Hisakuni, C.-H. Lin and S. Minakata, *Org. Lett.*, 2015, **17**, 318–321.
20 S. M. Walter, F. Kniep, E. Herdtweck and S. M. Huber, *Angew. Chem. Int. Ed.*, 2011, **50**, 7187–7191.
21 N. Schulz, P. Sokkar, E. Engelage, S. Schindler, M. Erdelyi, E. Sanchez-Garcia and S. M. Huber, *Chem. Eur. J.*, 2018, **24**, 3464–3473.
22 F. Zapata, A. Caballero, N. G. White, T. D. W. Claridge, P. J. Costa, V. Félix and P. D. Beer, *J. Am. Chem. Soc.*, 2012, **134**, 11533–11541.
23 A. Klamt and G. Schüürmann, *J. Chem. Soc. Perkin Trans. 2*, 1993, 799–805.
24 S. K. Khani, A. M. Khah and C. Hättig, *Phys. Chem. Chem. Phys.*, 2018, **20**, 16354–16363.
25 H. Miyasaka, K. Wada, S. Ojima and N. Mataga, *Isr. J. Chem.*, 1993, **33**, 183–192.
26 C. Chudoba, E. T. J. Nibbering and T. Elsaesser, *J. Phys. Chem. A*, 1999, **103**, 5625–5628.
27 G.-J. Zhao and K.-L. Han, *Acc. Chem. Res.*, 2012, **45**, 404–413.
28 J. Knorr, P. Sokkar, S. Schott, P. Costa, W. Thiel, W. Sander, E. Sanchez-Garcia and P. Nuernberger, *Nat. Commun.*, 2016, **7**, 12968.
29 J. Knorr, P. Sokkar, P. Costa, W. Sander, E. Sanchez-Garcia and P. Nuernberger, *J. Org. Chem.*, 2019, **84**, 11450–11457.
30 B. Dereka and E. Vauthey, *J. Phys. Chem. Lett.*, 2017, **8**, 3927–3932.
31 B. Dereka, I. Fureraj, A. Rosspeintner and E. Vauthey, *Molecules*, 2019, **24**, 4361.
32 Y. Lee, R. M. Malamakal, D. M. Chenoweth and J. M. Anna, *J. Phys. Chem. Lett.*, 2020, 877–884.
33 M. Head-Gordon, J. A. Pople and M. J. Frisch, *Chem. Phys. Lett.*, 1988, **153**, 503–506.
34 F. Weigend and R. Ahlrichs, *Phys. Chem. Chem. Phys.*, 2005, **7**, 3297–3305.
35 A. Hellweg, C. Hättig, S. Höfener and W. Klopper, *Theor. Chem. Acc.*, 2007, **117**, 587–597.
36 K. A. Peterson, D. Figgen, E. Goll, H. Stoll and M. Dolg, *J. Chem. Phys.*, 2003, **119**, 11113–11123.
37 F. J. O. D. Valle and J. Tomasi, *Chem. Phys.*, 1991, **150**, 139–150.
38 C. Hättig and F. Weigend, *J. Chem. Phys.*, 2000, **113**, 5154–5161.
39 J. Schirmer, *Phys. Rev. A*, 1982, **26**, 2395–2416.
40 C. Hättig, *Adv. Quant. Chem.*, 2005, **50**, 37–60.
41 *TURBOMOLE V7.2 2017, a development of University of Karlsruhe and Forschungszentrum Karlsruhe GmbH, 1989-2007, TURBOMOLE GmbH, since 2007; available from* `http://www.turbomole.com`.
42 F. Furche, R. Ahlrichs, C. Hättig, W. Klopper, M. Sierka and F. Weigend, *WIREs Comput. Mol. Sci.*, 2014, **4**, 91–100.
43 C. Boga, E. D. Vecchio, L. Forlani and P. E. Todesco, *J. Organomet. Chem.*, 2000, **601**, 233–236.
44 S. H. Jungbauer and S. M. Huber, *J. Am. Chem. Soc.*, 2015, **137**, 12110–12120.
45 M. Breugst, D. von der Heiden, E. Detmar and R. Kuchta, *Synlett*, 2017, **29**, 1307–1313.
46 F. Heinen, E. Engelage, A. Dreger, R. Weiss and S. M. Huber, *Angew. Chem. Int. Ed.*, 2018, **57**, 3830–3833.
47 G. R. Fleming, *Chemical Applications of Ultrafast Spectroscopy*, Oxford University Press, USA, 1986.
48 H. Lemmetyinen, N. V. Tkachenko, B. Valeur, J.-I. Hotta, M. Ameloot, N. P. Ernsting, T. Gustavsson and N. Boens, *Pure Appl. Chem.*, 2014, **86**, 1969–1998.
49 S. Schott, A. Steinbacher, J. Buback, P. Nuernberger and T. Brixner, *J. Phys. B*, 2014, **47**, 124014.
50 K. M. Mullen and I. H. van Stokkum, *J. Stat. Softw.*, 2007, **18**, (issue 3).
51 I. H. van Stokkum, D. S. Larsen and R. van Grondelle, *Biochim. Biophys. Acta – Bioenergetics*, 2004, **1657**, 82–104.
52 S. P. Laptenok, P. Nuernberger, A. Lukacs and M. H. Vos, *Meth. Mol. Biol.*, 2014, **1076**, 321–336.
53 A. D. Becke, *Phys. Rev. A*, 1988, **38**, 3098–3100.
54 S. Grimme, *WIREs Comput. Mol. Sci.*, 2011, **1**, 211–228.
55 N. M. Kreienborg and C. Merten, *Chem. Eur. J.*, 2018, **24**, 17948–17954.
56 K. Fukui, *Acc. Chem. Res.*, 1981, **14**, 363–368.
57 A. Hellweg, *Journal of Computational Chemistry*, 2013, **34**, 1835–1841.
58 Y. Marcus and G. Hefter, *Chem. Rev.*, 2006, **106**, 4585–4621.
59 B. Sauerwein and G. B. Schuster, *J. Phys. Chem.*, 1991, **95**, 1903–1906.
60 F. Ito and T. Nagamura, *J. Photochem. Photobiol. C*, 2007, 174–190.
61 P.-A. Bouit, C. Aronica, L. Toupet, B. Le Guennic, C. Andraud and O. Maury, *J. Am. Chem. Soc.*, 2010, **132**, 4328–4335.
62 A. C. Véron, H. Zhang, A. Linden, F. Nüesch, J. Heier, R. Hany and T. Geiger, *Org. Lett.*, 2014, **16**, 1044–1047.
63 J. N. Gayton, S. Autry, R. C. Fortenberry, N. I. Hammer and J. H. Delcamp, *Molecules*, 2018, **23**, 3051.
64 P. S. Pregosin, *Prog. Nucl. Magn. Reson. Spectrosc.*, 2006, **49**, 261–288.
65 P. G. A. Kumar, P. S. Pregosin, M. Vallet, G. Bernardinelli, R. F. Jazzar, F. Viton and E. P. Kündig, *Organometallics*, 2004, **23**, 5410–5418.
66 J. B. Birks, *Photophysics of aromatic molecules*, Wiley-Interscience, London, 1970.
67 V. Ramamurthy, J. C. Scaiano and N. J. Turro, *Modern Molecular Photochemistry of Organic Molecules*, Palgrave Macmillan, Sausalito, 2010.
68 N. B. Joshi, P. Gangola and D. D. Pant, *J. Lumin.*, 1979, **21**, 111–118.
69 N. Nijegorodov and R. Mabbs, *Spectrochim. Acta A*, 2001, **57**, 1449–1462.
70 K. N. Solov'ev and E. A. Borisevich, *Physics-Uspekhi*, 2005, **48**, 231–253.
71 P. Singhal and H. N. Ghosh, *Phys. Chem. Chem. Phys.*, 2014, **16**, 16824–16831.

Physical Chemistry Chemical Physics Accepted Manuscript

View Article Online
DOI: 10.1039/D1CP00009H

72 X. Niu, P. Gautam, Z. Kuang, C. P. Yu, Y. Guo, H. Song, Q. Guo, J. M. W. Chan and A. Xia, *Phys. Chem. Chem. Phys.*, 2019, **21**, 17323–17331.

73 A. L. Sobolewski and W. Domcke, *Chemical Physics*, 2000, **259**, 181–191.

74 A. L. Sobolewski and W. Domcke, *The Journal of Physical Chemistry A*, 2001, **105**, 9275–9283.

75 V. Vallet, Z. Lan, S. Mahapatra, A. L. Sobolewski and W. Domcke, *Faraday Discuss.*, 2004, **127**, 283–293.

76 O. P. J. Vieuxmaire, Z. Lan, A. L. Sobolewski and W. Domcke, *The Journal of Chemical Physics*, 2008, **129**, 224307.

77 M. Kadi, J. Davidsson, A. Tarnovsky, M. Rasmusson and E. Åkesson, *Chemical Physics Letters*, 2001, **350**, 93–98.

78 O. A. Borg, Y.-J. Liu, P. Persson, S. Lunell, D. Karlsson, M. Kadi and J. Davidsson, *J. Phys. Chem. A*, 2006, **110**, 7045–7056.

79 M. N. R. Ashfold, G. A. King, D. Murdock, M. G. D. Nix, T. A. A. Oliver and A. G. Sage, *Phys. Chem. Chem. Phys.*, 2010, **12**, 1218–1238.

80 M. Z. Zgierski, T. Fujiwara and E. C. Lim, *Acc. Chem. Res.*, 2010, **43**, 506–517.

81 J. Ammer, C. F. Sailer, E. Riedle and H. Mayr, *J. Am. Chem. Soc.*, 2012, **134**, 11481–11494.

82 K. E. Riley, J. S. Murray, J. Fanfrlík, J. Řezáč, R. J. Solá, M. C. Concha, F. M. Ramos and P. Politzer, *J. Mol. Model.*, 2011, **17**, 3309–3318.

Published on 09 March 2021. Downloaded by Ruhr Universitat Bochum on 3/9/2021 10:47:03 AM.

Physical Chemistry Chemical Physics Accepted Manuscript